Available online at www.sciencedirect.com
SCIENCE DIRECT
Tectonophysics 412 (2006) 121–140
TECTONOPHYSICS
www.elsevier.com/locate/tecto

Crustal thickening and variations in architecture from the Qaidam basin to the Qang Tang (North–Central Tibetan Plateau) from wide-angle reflection seismology

M. Jiang [a], A. Galvé [b,c,*], A. Hirn [b], B. de Voogd [d], M. Laigle [b], H.P. Su [a], J. Diaz [e], J.C. Lépine [b], Y.X. Wang [a]

[a] *Continental Dynamics Lab., Geological Institute, Chinese Academy of Geosciences, Baiwanzhuang road, 100037 Beijing, China*
[b] *Laboratoire de Sismologie Expérimentale, Department de Sismologie UMR 7580 CNRS, Institut de Physique du Globe de Paris, 4 place Jussieu, 75252 Paris Cedex 05, France*
[c] *School of Earth Sciences, Victoria University of Wellington, P.O. Box 600, Wellington, New Zealand*
[d] *Department Sciences de la Terre, MIGP UMR 5212, Université de Pau, 64000 Pau, France*
[e] *Institute of Earth Sciences Jaume Almera, Consejo Superior de Investigaciones Cientificas, calle Lluis Sole i Sabaris, Barcelona 08028, Spain*

Received 14 September 2004; received in revised form 9 September 2005; accepted 26 September 2005
Available online 6 December 2005

Abstract

Wide-angle reflection–refraction profiles at crustal scale have been obtained along a 700 km transect of northeastern Tibet from six shotpoints. A combination of sampling by broadside fan-recordings and in-line profiling allows us to image increases in Moho depth towards the centre of the plateau. These occur with different styles across the two block boundaries between North Kun Lun, Bayan Har and Qang Tang, as shown also by the changes resolved in the internal architecture and layer velocities in the crust. Clear S-waves are observed: together with P-waves they bring rare constraints on the composition of crustal units, which reveals an abnormally felsic average composition for the whole crust and its lower half along the whole length of the transect.

Across the North Kun Lun–Qaidam block, variations of crustal thickness are detected, with Moho depth between 55 and 65 km, and an inverse correlation with basement topography. In the north of the Bayan Har block, a strong heterogeneity in the middle of the 70 km thick crust is shown. As suggested from synthetic seismograms modelling, it may result from thin layer inclusion marking the northward tectonic superposition of the Bayan Har crust on the North Kun Lun crust. As imaged by a fan profile, the corresponding upper part could have been transported northwards to thicken also the upper crust of the present North Kun Lun block. In the north of Qang Tang, a model is obtained with a 75-km thick crust and a lower half of the crust with average velocities characteristic of felsic composition. From Bayan Har to Qang Tang, variations of deep architecture are documented across the Jinsha suture and Xianshuihe fault from recording in-line and broadside to several shotpoints. Together with the felsic composition of the lower part of the crust, a Moho offset suggests the imbrication of the Bayan Har crust in the Qang Tang lithosphere between a south-dipping Moho above and a north-dipping Moho below. A model of indentation of the Qang Tang by an originally thinner Bayan Har crust and lithosphere, with part of the Qang Tang

* Corresponding author. Department Sismologie, Case 89, Institut De Physique Du Globe De Paris, 4, Place Jussieu. 75252 Paris Cedex 05, France. Tel.: +33 1 44 27 39 14; fax: +33 1 44 27.
E-mail address: galve@ipgp.jussieu.fr (A. Galvé).

0040-1951/$ - see front matter
doi:10.1016/j.tecto.2005.09.011

brought to greater depth would also be consistent also with the Moho topography across the transition from the Qang Tang to Bayan Har, as imaged by fan profile.

Keywords: Tibet; Explosion seismology; Seismic velocity; Seismic attenuation; Crustal structure; Composition

1. Introduction

Spatial variation of the thickness and internal structure of the crust across regions of present active convergence can be resolved by reflection–refraction seismic methods. Such an image of the result of the evolution of the continental lithosphere provides constraints on the processes and mechanisms of material deformation and transport. The northeastern edge of Tibet, where the crust is presently experiencing thickness processes (Meyer et al., 1998), could be sampled at crustal scale by a wide-angle reflection and refraction seismic experiment. On the main SSW–NNE transect that is 700 km long from the Qang Tang block in Central Tibet, through the Bayan Har block and into the North Kun Lun–Qaidam block (Fig. 1), were recorded three of the 3- to 5-ton shots detonated in borehole arrays in order to compose a 2D model. Additional in-line and fan profiles were obtained, with the over 200 recorders displaced each once or twice during the 3-week survey of 1998, to test spatial variations.

The continental crustal block of the North Kun Lun–Qaidam shows a succession of ranges and of intermountain basins such as the Qaidam, Gonghe and Qinghai basins (Fig. 1). The largest one, the Qaidam basin, has an elevation as low as ~2800 m amidst borders over 5000 m high, and a sediment infill estimated to be up to 10 km thick (Métivier et al., 1998; Chen et al., 1999). The next block to the south, the Bayan Har block, also called Songpan–Garze terrane is considered to have originated as a continent–ocean margin with a 5 to 10 km thick cover of Triassic flysch. This cover was fed from the Qinling Orogen that was formed to the east when at Late Triassic, the North and South China blocks collided (e.g., Mattauer et al., 1992; Bruguier et al., 1997). The Qang Tang block of continental crust to the south forms the centre of the Tibetan Plateau. The three blocks described above sutured along the Triassic Kun Lun suture and the Jurassic Jinsha suture. These sutures have been successively re-activated from south to north after the collision of India, setting up the left-lateral strike-slip Xianshuihe and Kun Lun faults. From the geological study of this region a model of plateau formation by stepwise growth has been proposed by Tapponnier et al. (1990, 2001) and Meyer et al. (1998).

In the northern half of Tibet, previous studies of deep structure have reported a moderately thickened crust, over 1000 km away from the Himalayan convergence zone, from teleseismic P-wave tomography (Wittlinger et al., 1996) and from teleseismic S to P converted waves (Owens and Zandt, 1997). However the thickness and the internal structure of the crust, which mark its mode of evolution, may be better resolved by high-frequency waves from artificial sources and the tight spatial sampling in refraction–reflection seismology. In the southern Qang Tang and into the Lhasa blocks, Zhao et al. (2001) carried out such an explosion seismology transect across the structural strike, with several shotpoints over 450 km. From a 2D modelling of P waves they report a crust of 65-km thickness with a main mid-crustal interface without notable variations.

The present explosion seismology survey contrasts with the standard approach in three ways. First of all the spatial sampling is improved by shooting and recording not only along but also broadside to the transect. Profiles were specifically designed outside the 2D dip-line transect, as in-line or fan profiles, in order to check the regional variations of features detected on the transect, giving thus control on the intracrustal and Moho architecture. Second, the use of 2 Hz sensors allowed us to record signals in presence of a significant attenuation which prevented high frequencies generated by the explosive shots to propagate very far. Third, clear S-waves could be recorded in addition to P-waves, since 3-component sensors were used.

Galvé et al. (2002a) illustrated that there were first-order contrasts between crustal blocks. According to them, the crustal architecture across the limit between the North Kun Lun–Qaidam and Bayan Har blocks suggests imbrication and the thickened crust of North Kun Lun–Qaidam is felsic.

In this study we document new elements on the architecture at the northern edge of the Qang Tang towards the Bayan Har block, which have implications on evolutionary models. They suggest lithospheric imbrication at diverse level, which can be viewed as partial collision or subduction. However, these mechanisms

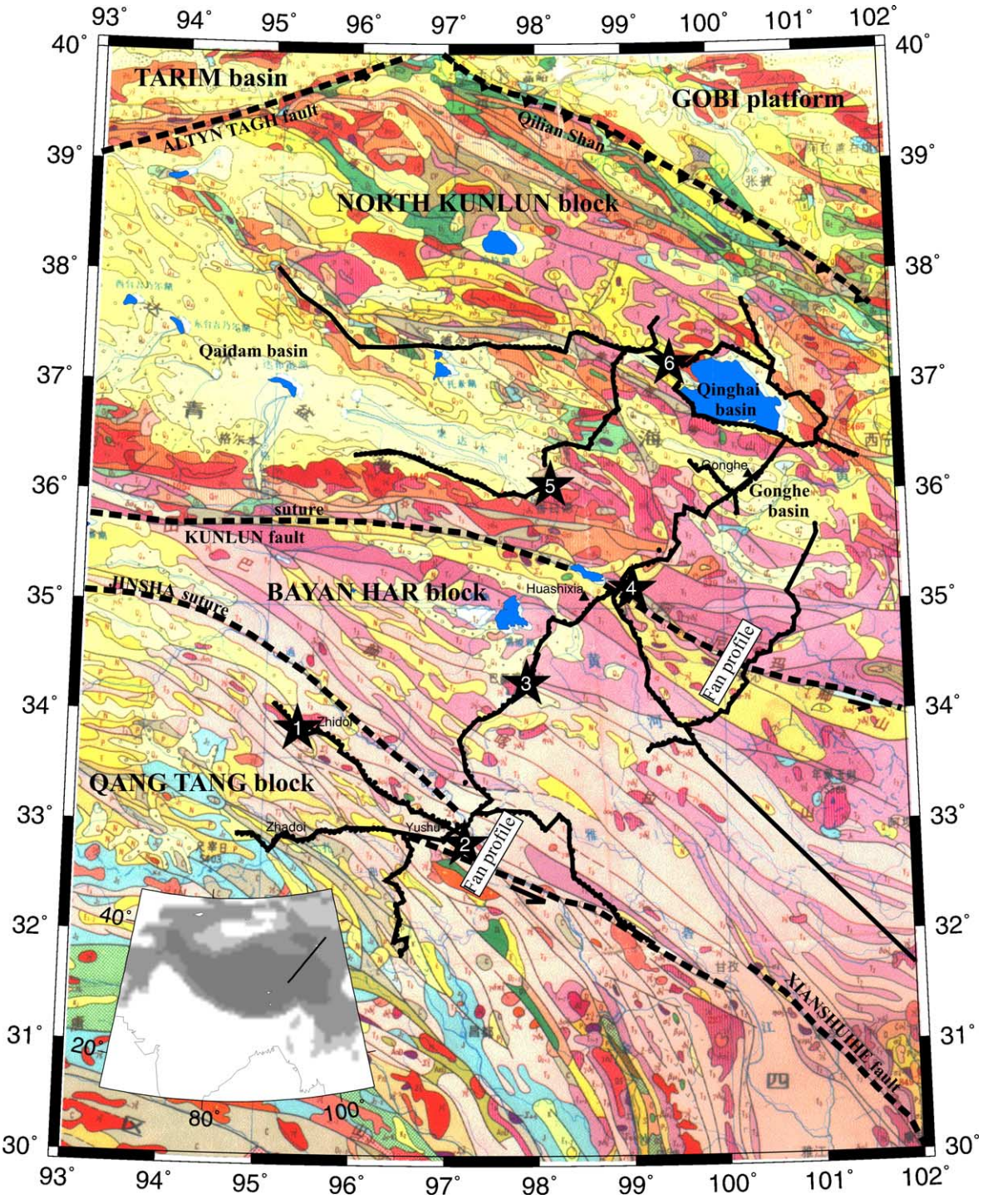

Fig. 1. Geological map of the northeastern part of the Tibetan plateau showing in yellow: Eocene to Quaternary rocks; in green: Cretaceous rocks; in blue: Jurassic rocks; in pink: Triassic rocks and in red: metamorphic rocks and granite. Black stars are shotpoints of charges of 3 to 5 tons. Black lines represent the profiles with 3-component seismometers at 5 km spacing.

involved at the northern edge of the Qang Tang appear to be different to the ones observed at the northern edge of the Bayan Har (Galvé et al., 2002a). We also constrain V_p/V_s in the Bayan Har and north Qang Tang. This allows us to suggest a tentative interpretation of elastic parameters of the lower half of the crust in northern Qang

Tang and northern Bayan Har. They appear to be similar in composition but with different metamorphic facies. Galvé et al. (2005—this issue) develop further inferences on temperature, hydration and evolution of the lower crust from additional constraints on seismic attenuation derived from joint elastic and anelastic modelling of amplitudes.

2. Data set and modelling practice

The six shots have generated P-waves that can be correlated consistently over several tens of kilometres along the line of stations; it attests to the presence at depth of reflecting levels with reasonable continuity. Several traveltime curves can be correlated on each record-section in each block, notably the PmP reflection from the crust–mantle boundary (Fig. 2). A first order difference among the three crustal blocks is their contrasted reflectivity response (Galvé et al., 2002a). While the North Kun Lun–Qaidam sections reveal a simple structure with a strong Moho reflection, the Bayan Har block shows successive branches of traveltime curves and among them a mid-crustal reflection that is strong with respect to the Moho reflection. In the Qang Tang block also several traveltime curves are seen and the Moho reflection appears strong and clear at offsets that are short with respect to its late arrival time.

Velocity–depth models have been constructed by trial and error modelling (Zelt and Smith, 1992), in order to provide traveltimes matching the observations. Due to the trade-off on traveltime between interface depth and layer velocity, there is a well-known non-uniqueness, with not only a range, but possibly different types, of acceptable models. The strategy adopted is to obtain for each record section first a minimum-structure model. This is the simplest model, in which there are not more interfaces than traveltime curve branches, and the velocity increases stepwise at interfaces. In addition, a 2D model is then derived from these 1D models on the main SSW–NNE transect. Consistency of overlapping observations among shots recorded on a line or crossing lines is checked during this process.

Then, amplitudes are considered, in particular the location of the maximum of the amplitude along the profile, and the relative amplitude level on successive branches. These amplitudes are compared to those of synthetic seismograms generated by the reflectivity method (Fuchs and Mueller, 1971; Kennett, 1975) for a variety of tentative models. Even though P-waves are the focus of such an explosion seismic study, the use of low-frequency, three components seismometers allowed the observation of S-waves, that contribute unique indications on the composition of the north Tibetan crust.

3. Simple velocity–depth model and lateral variation of the crust in the North Kun Lun–Qaidam block

Galvé et al. (2002a) have reported from coincident S and P reflections that the composition is felsic on average for the whole thickness of the crust in the North Kun Lun–Qaidam block. They inferred that thickening of mostly the upper crustal layer led to an anomalous crustal thickness. Here, by considering additional profiles, the lateral variations in crustal thickness within the block can be resolved and intracrustal layering discussed. It was sampled by three of the six shots. In addition to the main North–South line, groups of stations were placed on the borders of the Qinghai and Qaidam basins (Fig. 1). In this way, reflections from deep interfaces beneath the basins could be recorded, avoiding the effects of the thick and not well-known sedimentary layer in particular the delay introduced on arrival times. The main feature is a strong and clear Moho reflection after few weak intracrustal reflections (Fig. 2). Lateral contrasts are clearly evidenced since the Moho reflections at a same distance on different record-sections have different arrival times and different slopes. This reflects strong variations in the upper lithosphere across the Qaidam–North Kun Lun block. A significant variation of the Moho depth is implied in case the average crustal velocity does not vary over the region.

3.1. Lateral variation in crustal thickness, rather than velocity in the North Kun Lun–Qaidam block

Moho reflections are very clear on most record-sections, but the intracrustal arrivals are weak, indicating small velocity contrasts as compared to the one corresponding to the Moho discontinuity. An assessment of uncertainty in average crustal velocity and

Fig. 2. Examples of record-sections (represented with a 6 km/s velocity reduction) highlighting the different reflectivity response of the three blocks crossed, as discussed in the text: a) Shot 6 to west, b) Shot 5 to northwest, in the North Kunlun–Qaidam block characterized by a clear and strong Moho reflection PmP (T5). c) Shot 4 to southeast, d) Shot 4 to southwest in the Bayan Har block, where a strong intracrustal reflection T5 is seen in addition to the Moho reflection, T7. e) Shot 2 to northwest in the Qang Tang block, the Moho reflection T6 is strong at short offset despite its late arrival time.

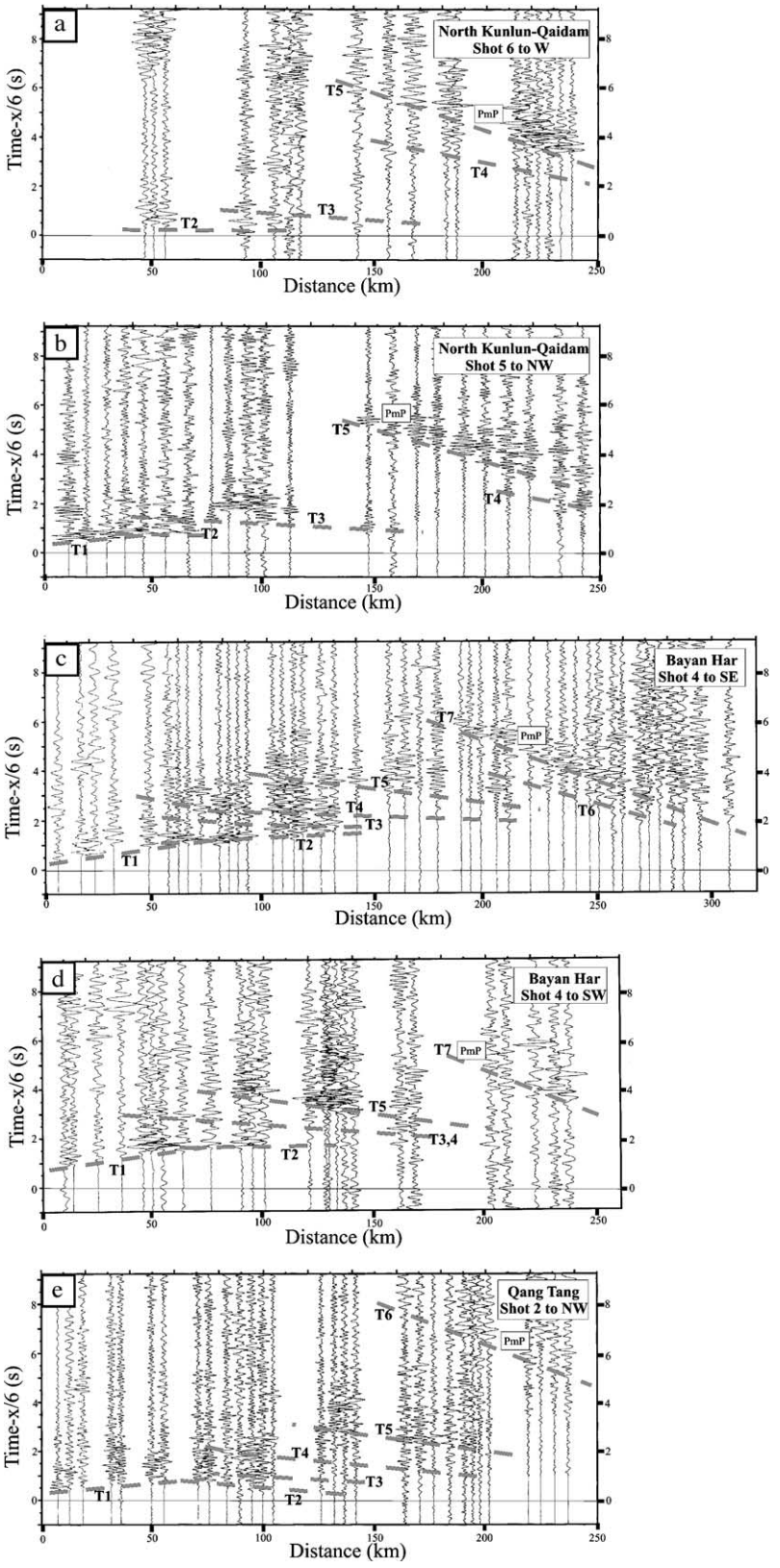
a
North Kunlun-Qaidam
Shot 6 to W
T5
PmP
T4
T3
T2
Time-x/6 (s)
Distance (km)
b
North Kunlun-Qaidam
Shot 5 to NW
PmP
T5
T4
T3
T2
T1
Time-x/6 (s)
Distance (km)
c
Bayan Har
Shot 4 to SE
T7
PmP
T5
T4
T3
T6
T2
T1
Time-x/6 (s)
Distance (km)
d
Bayan Har
Shot 4 to SW
T7
PmP
T5
T3,4
T2
T1
Time-x/6 (s)
Distance (km)
e
Qang Tang
Shot 2 to NW
T6
PmP
T5
T4
T3
T2
T1
Time-x/6 (s)
Distance (km)

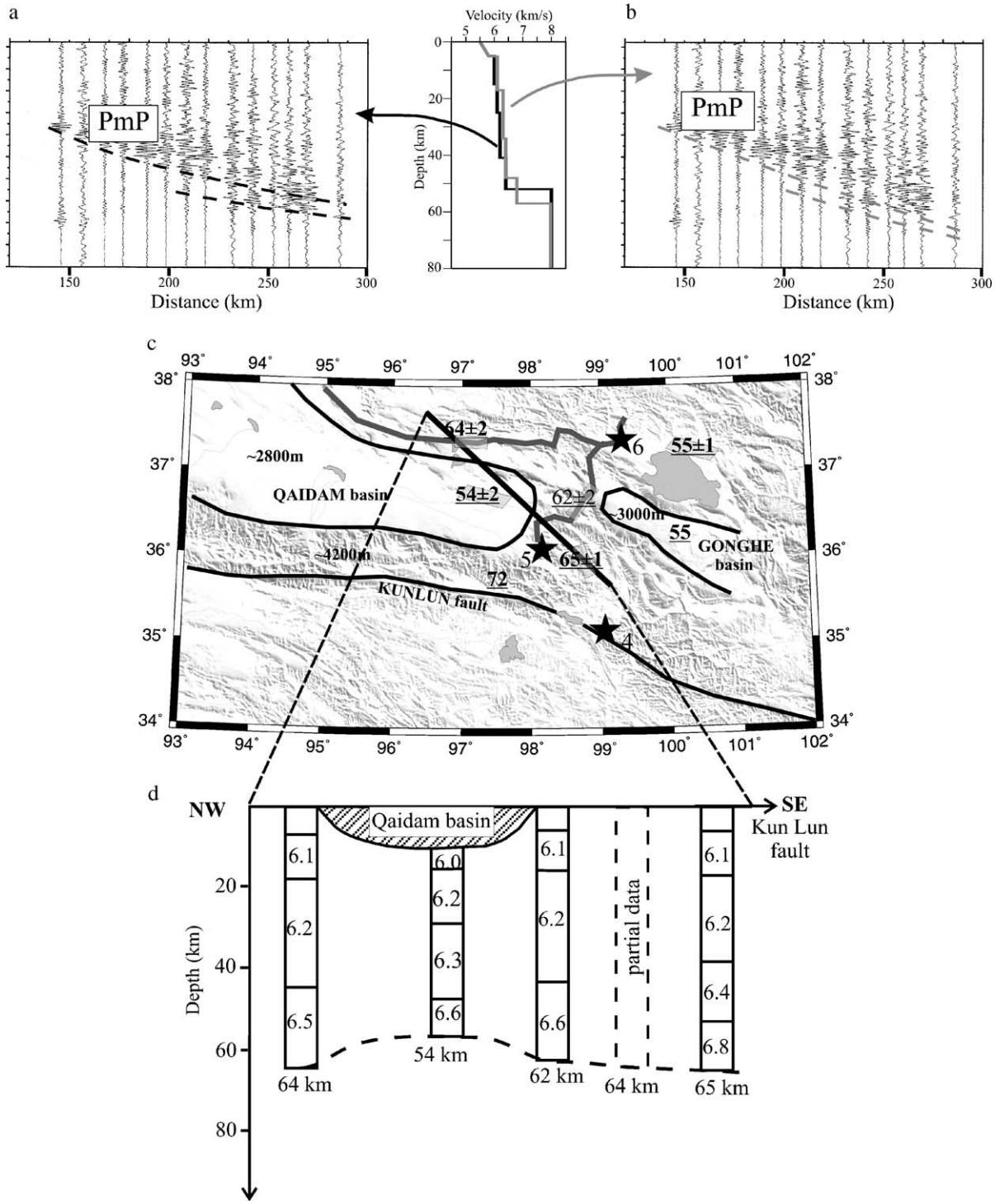

Fig. 3. Moho depth and crustal structure obtained in the North Kunlun–Qaidam block, an example from Shot 5 to northwest. a) and b) Two different and extreme choices of PmP correlations and corresponding velocity–depth models in black and grey still fitting the same observations as displayed with the corresponding different correlations of traveltime curves for the last deep intracrustal and the Moho reflections. c) Crustal thickness values in map view as sampled by the several profiles. d) Crustal columns with values of velocities in km/s, projected along the black line just above, showing the less thickened crust under the Qaidam basin.

thickness is given in the next section and illustrated in Fig. 3a and 3b. From the correlated traveltime branches such as in Fig. 2a and b, velocity–depth models are developed as in Fig. 3d, and the spatial variation of Moho depth summarized in Fig. 3c.

For the sake of completeness, we describe the correlations adopted, the resulting velocities and thicknesses and their spatial variability. Although shotpoints are located in basement rocks of different geological units, record-sections (Fig. 2a and b) do not show any strong variation in the upper crust structure. The closest stations sample an upper layer of 5–6 km thickness with a velocity gradient, from around 5.6 to 5.9 km/s (Fig. 3b). The amplitude and critical distance of the two next traveltime curves (T2 and T3) can be fitted in both the sections by reflections at the base of layers with 6.1 and 6.2 km/s velocities. With this same value of the velocity for both profiles, the base of the 6.2 km/s layer appears then to be deeper south of the Qaidam basin than north of it. The interface is 29 km deep below the surface of the Qaidam basin, and 38 km deep south of it. The best fitting velocity in the next layer obtained by modelling the T4 traveltime curve, varies from 6.3 km/s in the north to 6.5 km/s in the south whereas the depth of its base increases from 45 to 53 km.

The lower crustal layer beneath is only about 10 km thick, as derived from the last traveltime curve (T5) which corresponds to the reflection from the crust–mantle boundary. Its velocity is 6.5 km/s north of the Qaidam, 6.6 km/s under the Qaidam and 6.8 km/s south and east of it, although these differences in velocity are not well constrained since the lower crustal layer is thin. The whole crustal thickness under the Qaidam basin appears thinner (54 km) than under its margins where we observe 64 km to the north, 62 km to the east and 65 km to the southeast of the basin. The profile north of the Qinghai Lake shows that the crust has a 55 km thickness and an average velocity of 6.3 km/s.

In order to sample the Moho depth in more locations, groups of stations were placed at different azimuths from shotpoints at the expected critical distance. Then, using the shallower part of the velocity–depth model of the nearest profile, we have modelled the observed traveltime curve of the deeper interfaces (T4 and T5). On the southern border of the Qaidam basin, we found a crustal thickness of 72 km and an average velocity of 6.3 km/s. This is an indication that the Moho is deeper towards the Kun Lun suture. We obtain also a value of 64 km on the eastern border of the Qaidam basin. Another measurement obtained just south of the Qinghai basin yields a thickness of only 55 km (Fig. 3c and d).

3.2. Resolution of lateral variations

To check that the data from different profiles can resolve these differences in crustal velocity and Moho depth, we estimate the errors bars on the velocity–depth models. We do this by keeping a similar minimum-structure model and searching for the extreme values of layer velocity and corresponding thickness, which still allow fitting of the observed traveltime curves. Fig. 3a illustrates on an example the accuracy on thickness and velocity for the layer above the crust–mantle boundary, as constrained by the last traveltime curve (T5). The recording of shot 5 from stations north of the Qaidam basin gives a record-section that samples the Moho under the Qaidam basin. Since the reflection is observed over a long distance range, there is only a narrow range of velocity values that allow us to fit the traveltime curve. The case here is extreme since we incorporate the possibility of misinterpretation, with a different wave correlation for T5 as shown in the two sections of Fig. 3. Even though, it is only by changing by 0.2 km/s the 6.6 km/s velocity value in the lowest part of our preferred model that the slope of the computed traveltime curve deviates from fitting the furthest offsets observed arrival times. In this worst case, we still have a constraint on the average crustal velocity of ± 0.06 km/s and on the thickness of ± 2 km.

This small error bar, allows us to be confident in the large Moho depth variations found in the North Kunlun–Qaidam. Since the sedimentary infill of the Qaidam basin is estimated to be around 10 km thick (Chen et al., 1999; Métivier et al., 1998), the thickness of the non-sedimentary crust under the Qaidam basin is then of 45 km, significantly less than the values of over 60 km on its borders. Under the Qinghai lake the thickness of the sedimentary layer is not well known but in any case the total crustal thickness with the sediments is 55 km, that is smaller than under its border where we found 60 to 65 km (Fig. 3d).

4. The Bayan Har block: alternating low or high velocity layers and crustal architecture at its northern edge

4.1. A minimum structure model is not sufficient

In contrast to the previous record-sections in the North Kun Lun–Qaidam block, in the Bayan Har block several intracrustal reflections can be correlated

(Fig. 2c and d). Notably, a main intracrustal reflection T5 observed from 100 to 200 km at the reduced time of 3 to 4 s is characterized by a strong amplitude. This strong mid-crustal reflection appears on all the record-sections from the Bayan Har block. However there are some differences in the characteristic of the deeper reflections: an additional traveltime curve T6 can be correlated before the Moho reflection, as in Fig. 2c, or not, as in Fig. 2d.

Fig. 4b displays the synthetic seismograms for a model of the Bayan Har sections in Fig. 2c and d, with the same number of interfaces as observed reflected traveltime branches for Shot 4 towards the southwest (Figs. 2d and 4a). We successfully fit the amplitudes of the first traveltime curves T1, T2, T3 and T4, the traveltime branches T1 and T2 being consistent with respectively refraction and reflection of a 5 to 8 km thick layer of metamorphic flysch expected in the Bayan Har (Mattauer et al., 1992).

However, this minimum-structure model constructed to fit the arrival times does not fit satisfactorily the amplitudes of the last traveltime curves, nor does any model of the same kind explored in the trial and error modelling. The high amplitude of the strong mid-crustal reflection in the observed data at a short offset of 140 km with respect to the amplitude of the Moho reflection cannot be obtained on the synthetics. This is true even when here as in the following, a high velocity value of 8 km/s is assumed in the upper mantle. Velocity–depth models with more complex structures are indeed necessary for the deeper part.

4.2. Alternative velocity–depth models for the strong amplitude intracrustal and Moho reflections: possible tectonic superposition of crusts at the northern edge of Bayan Har

On the synthetic seismograms of the minimum-structure model (Fig. 4b) the strong amplitude and the short critical distance of the T5 reflection could not be fitted with a single layer of velocity over 6.8 km/s down to the Moho, beneath the 6.3 km/s velocity above. This is because if material with such velocity reached down to the Moho, the reflectivity of the latter would not give the appropriate amplitude level and amplitude versus offset variation. We shall explore non-minimum-structure types of crustal models containing hidden layers, such as low velocity layers, that is models with more interfaces than traveltime curves observed.

In a first type of model, we test a low-velocity layer on top of the mid-crustal interface, in order to move the amplitude maximum to shorter distance and increase the amplitude of the T5 reflection. With a velocity step from 5.8 to 6.9 km/s at 31 km depth, the strong intracrustal reflection together with the Moho reflection are then fitting observations from shot 4 towards the southeast (Fig. 4c). There is no strong constraint on the thickness of the 5.8 km/s material under the 6.2 km/s one since there is no wide-angle observation of the top of the low-velocity layer, and hence the depth of the interface at its base is not precisely determined. The value of the average velocity in the lower part of the crust may vary from 6.9 to 7.1 km/s from one profile to the other, depending on the observed critical distance of the Moho reflection that is around 230 to 210 km, respectively. This lower layer of the crust is 40 km thick, except for the profile of Shot 3 towards the north, whose stations are situated north of the Kun Lun fault. Here we have a smaller thickness of 30 km for the lower crust, and a total crustal thickness around 72 km.

In the other type of model, we increase the velocity of the layer underneath the 6.2 km/s layer at 33 km depth (Fig. 4d). To fit the amplitudes, the velocity under the interface has to be increased up to 7.6 km/s, a value close to that in the upper mantle. In this type of model, the velocity has then to decrease again at some depth beneath that interface, in order to allow modelling the amplitude level and critical distance of the next branch that is the reflection from the Moho. In the corresponding lower crustal low-velocity layer, the velocity value has to be at most 6.8 km/s to fit observations. As usual, the thickness of the high-velocity inclusion under the mid-crustal reflector is not well-constrained. Fig. 4d displays the synthetic seismograms and the corresponding velocity–depth model with a 70 km

Fig. 4. Bayan Har (Shot 4 towards SW in Fig. 1). Observed and synthetic seismograms for different velocity–depth models, represented with a 6 km/s velocity reduction and amplitudes scaled with distance. a) Observed record-section, with the strong intracrustal reflection T5 and the Moho reflection T7. b) Minimum structure model with layers of increasing velocity with depth accounting for traveltimes where observed. It does not allow to fit the amplitude and critical distance of the intracrustal reflection T5. c) First option of a low velocity layer on top of the intracrustal interface, in order to increase the velocity contrast, thus fitting better amplitudes of T5. d) Second option, of a high velocity layer under the intracrustal interface in order to increase the velocity contrast, and consequently a deeper low-velocity layer on top the deep Moho in order to restore the velocity contrast there, thus fitting better amplitudes. These simplified 1D model do not imply there is a thin layer continuous under the whole profile.

thick crust that includes a 7.6 km/s velocity layer at around 35 km depth followed by a 30 km thick 6.8 km/s velocity layer for the lower crustal part.

Even if the observed record-sections show the same main characteristics, in detail the record-section amplitudes appear to be explain either by the mid-crustal

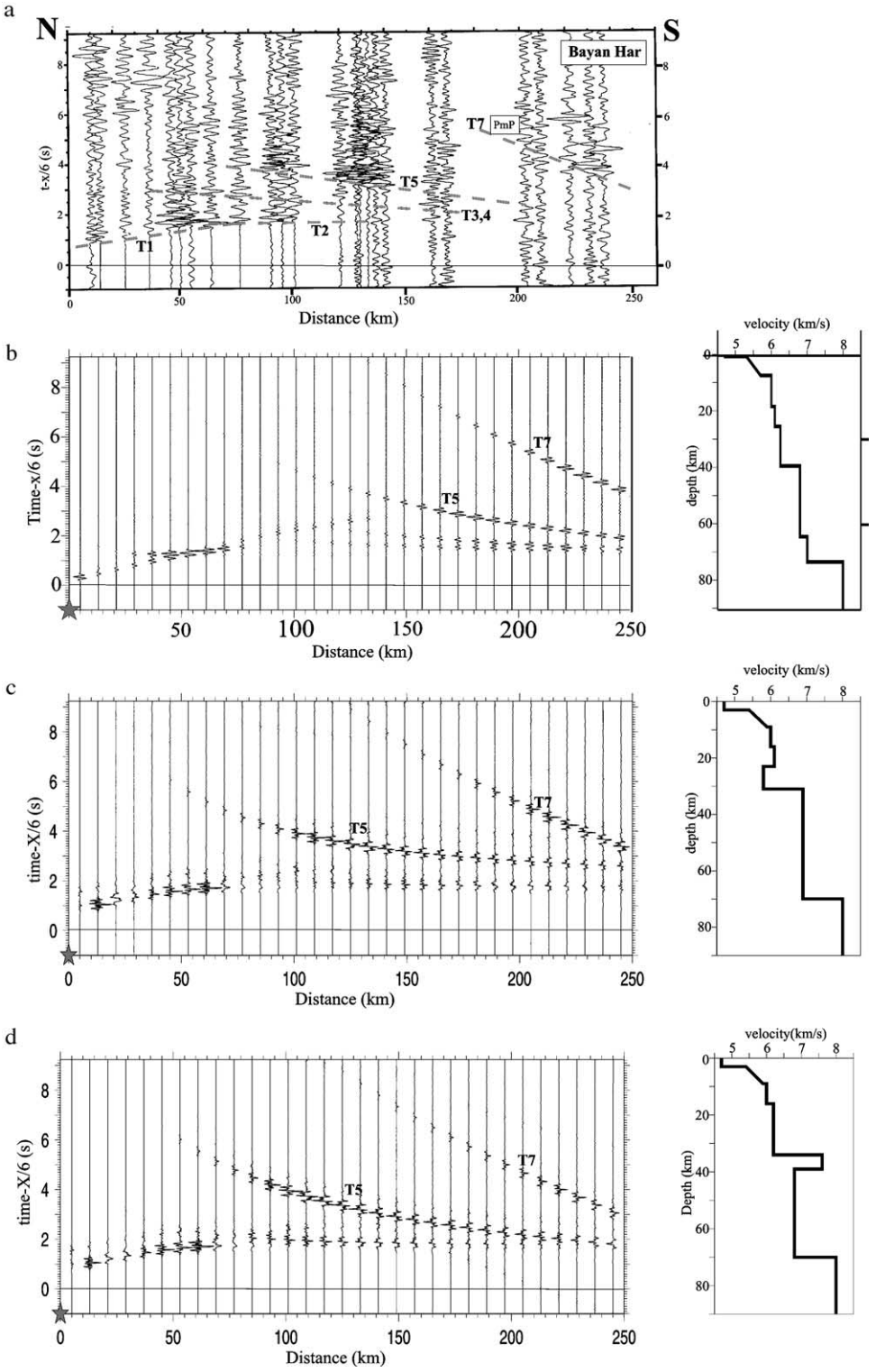

high velocity layer or by the mid-crustal low velocity layer types of models.

The two types of velocity–depth models that are found to account for the observations coincide in their crustal thickness that is the same, on the order of 70 km, much thicker than normal. This reveals that the present high surface topography of the Bayan Har terrane is supported by a crust that has been thickened rather than by a local upper mantle heterogeneity.

4.3. V_p and V_p/V_s, composition and possible anisotropy

Clear S-wave Moho reflections (SmS) allowed us to constrain an average $V_p/V_s = 1.73 \pm 0.01$ (Galvé et al., 2002a) in the North Kun Lun–Qaidam block. This is significantly lower than the average for a continental crust, which is 1.77 to 1.78 according to Christensen and Mooney (1995) and Zandt and Ammon (1995). It hence documents an average felsic composition for the whole thickened crust. By contrast, the SmS reflection is usually poorly recorded in the Bayan Har block, SmS is instead not seen in general. The exception is for Shot 3 recorded towards the northeast, where S waves could be recorded into the North Kun Lun block possibly because of better propagation there (Fig. 5). These arrivals can be used to estimate Vs. under the Bayan Har where the rays bottom. Here at least two traveltime curves can be correlated on the S-waves section that will allow us to resolve the value

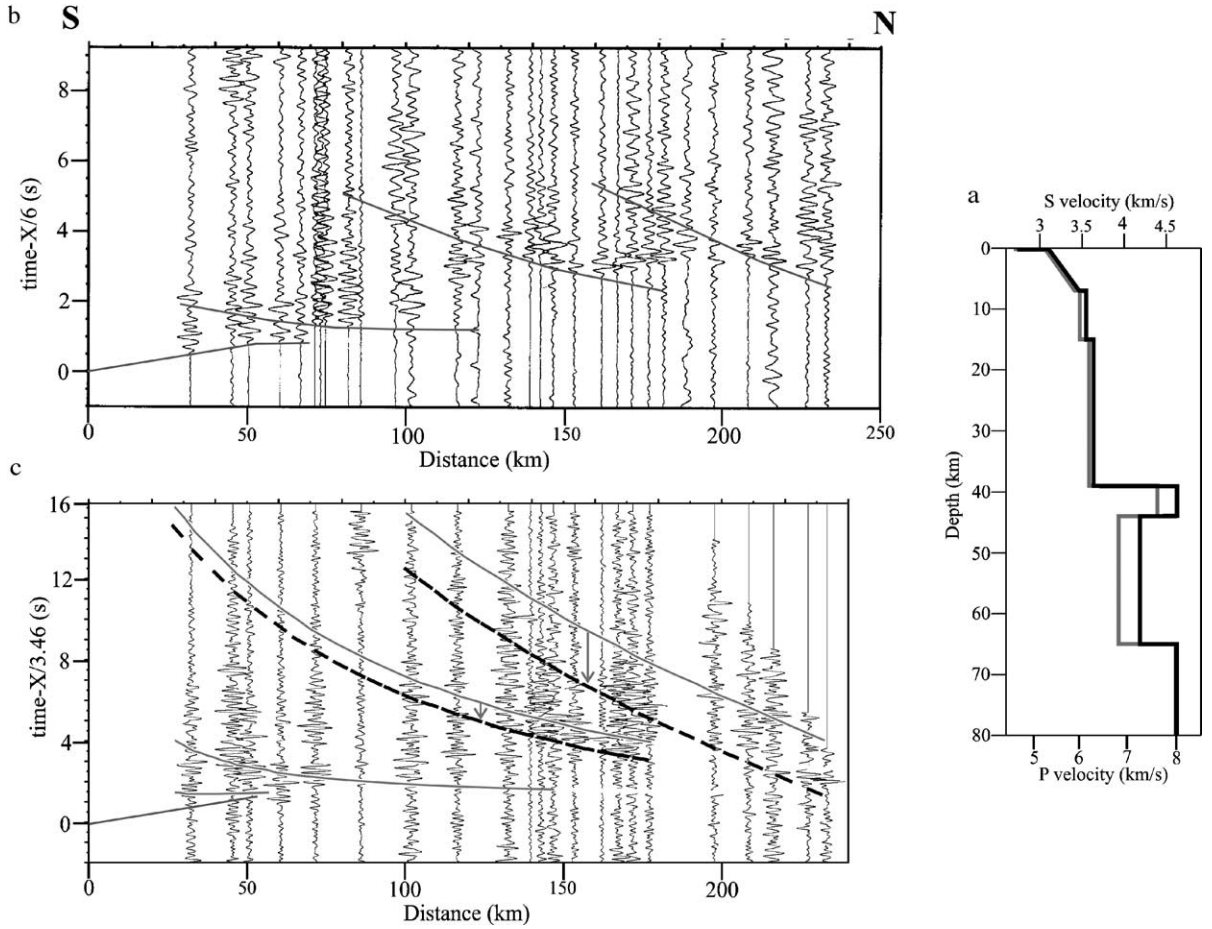

Fig. 5. Constraint on the V_p/V_s ratio in the Bayan Har block. Shot 3 towards NE. a) Velocity–depth model in grey for the P-waves and in black for the S-waves. b) P-waves record-sections on which the traveltime curves of the velocity–depth model are superimposed in grey. Between 170 and 200 km, we have a poor correlation between the traveltime curve of the velocity–depth model and the observed arrivals that is due to the use here of 1D velocity modelling. These arrivals are well fitted in 2D modelling by the presence of a thick sedimentary basin beneath the stations (Fig 8). c) S-waves record-section represented assuming V_p/V_s ratio equal to 1.73 for time scale and reduction velocity, in order to be directly comparable with the P-waves record-section. The P traveltime curves of b) have been superimposed in grey full line. The black dashed lines represent the S-wave arrival time correlations. The earlier arrival of the S-wave implies a lower V_p/V_s ratio in the lower part of the velocity–depth model, as illustrated in the corresponding velocity–depth models of a), grey for P and black for S.

of V_p/V_s in the layers between the reflecting interfaces, and not only derive a crustal average as in the North Kun Lun where the intracrustal reflections were weak. When we plot on the S section the S-wave traveltimes predicted from the P velocity–depth model by assuming a 1.73 velocity ratio (Fig. 5), S arrivals are observed earlier, hence the V_p/V_s ratio is lower than 1.73.

S arrivals even get relatively earlier with respect to the model derived from P, from one traveltime branch to the later. Hence the V_p/V_s ratio is decreasing with increasing depth, and is smallest for the lower crust. Modelling the S velocity with depth by assuming the layer thicknesses derived from P, then results in a V_p/V_s value of 1.70 for the layer at mid-crustal depth from 15 to 39 km and a value of 1.63 for the lower part of the crust from 39 to 65 km depth. This velocity–depth modelling assumed the same structure all along the profile. However the propagation is not completely in the Bayan Har, but also in part in the North Kun Lun block. Since in that block the average crustal velocity ratio has been derived as 1.73 (Galvé et al., 2002a), the values obtained here are upper bounds on the values for the Bayan Har.

An interpretation of such small V_p/V_s values may be sought in a peculiar composition or possible anisotropy. Considering measurements on rock samples, a way to account for low V_p/V_s is to consider that crustal composition is felsic on average, with a large proportion of quartz and albite as the plagioclase feldspar (Christensen, 1996). Thus felsic rocks as a granite–gneiss have a velocity of 6.3 km/s and $V_p/V_s=1.70$ (Kern and Richter, 1981; Christensen, 1996). However, the values we measure are in situ values at depth that depend on pressure and temperature. With temperature increasing with depth, V_p and V_p/V_s of quartzite and granite show strong variations. First, there is a significant decrease, when temperature increases from 200 to 500 °C, due to the quartz alpha to beta transition, then there is a drop in V_s at melting (Kern, 1982; Müller and Raab, 1997). Depth makes velocities vary also due to their pressure derivative, but pressure–temperature changes may also induce changes in metamorphic facies. The effects of both pressure and temperature on the rock velocities, but also the possibility of phase transitions have been considered by Sobolev and Babeyko (1994) in their petrophysical modelling of rocks from monomineral parameters. They find a very distinct drop of V_p/V_s with increasing pressure, in an isothermal transition from low-pressure to high-pressure facies. For instance at a temperature of 700 °C, V_p/V_s in granite decreases from 1.69 to 1.64 when pressure increases from 1.2 to 1.8 MPa, and V_p/V_s in diorite decreases from 1.76 to 1.69 between 0.8 and 1.5 MPa. For a granodiorite with an intermediate composition, and thus a more realistic V_p with respect to our estimation for the lower crust at the northern edge of Bayan Har (6.8 km/s), V_p/V_s would decrease from 1.70 at 0.8 MPa to 1.66 at 2 Mpa, whereas V_p increases from 6.3 to 6.8 km/s. The observation of a low value for V_p/V_s that is decreasing with increasing depth may thus be interpreted as due to the material being of felsic composition even at the great depth of the lower crust under the Plateau.

On the other hand, S-velocity peculiarities in the crust have been inferred in the Bayan Har from teleseismic receiver-function analysis. Transverse component energy, together with a variation of the radial as a function of backazimuth have been noted and attributed to conversion at a dipping intracrustal S low velocity layer by Zhu et al. (1995) and Owens and Zandt (1997). Vergne et al. (2003) also detect this phenomenon specifically along the routes followed by seismic profile presented here, but attribute it instead to shear-wave splitting in an anisotropic layer of schists in the upper crust between 10 and 18 km depth. Their model contains a layer of transversely isotropic material, anisotropic material having a hexagonal symmetry, with the slow velocity along the axis of symmetry, which they model as striking N40°E with a 40° dip. This strike is that of the present explosion seismology profile and propagation direction, and this dip is just the ray incidence for deep crustal critical reflections. The downgoing ray from the shot point in the Bayan Har recorded NE on the North Kun Lun–Qaidam block would then be along the axis of symmetry of such an anisotropic layer, propagating with the lowest value of S-velocity, as well as the lowest value of P-velocity. Therefore, the measurements of P and S velocities is unperturbated by the anisotropic fabric. Hence, even if such an anisotropic layer existed, the derived V_p/V_s ratio along the explosion seismology profile is representative of the composition of the material (e.g., Godfrey et al., 2000) which would not be the case at other incidences since the velocity of P and S waves will be affected by anisotropy.

Such anisotropy is hence no explanation to the abnormally low V_p/V_s observed in wide-angle crustal reflections. However the possible presence of another type of anisotropy and its effect on the V_p/V_s ratio needs to be considered. Hirn et al. (1995, 1997, 1998) by considering teleseismic S and P delays and S splitting delays along the line from the Himalayas into Qang Tang, documented that anisotropy in the upper mantle and in the crust was not of the simple type usually

considered in SKS-splitting studies. Anisotropy appears there with orthorhombic symmetry rather than with a horizontal symmetry axis, that is merely an azimuthal anisotropy in the horizontal plane as has only been considered there by Sandvol et al. (1997), Chen and Özalaybey (1998) and Huang et al. (2000).

This is constrained by observations otherwise unaccounted for, such as i) the dependence on incidence, shown by a splitting delay larger for S waves than for SKS waves, and ii) the increase from Himalayas to Qang Tang, together with this splitting delay, of a delay of first arrivals of teleseismic S out of proportion with respect to that of P, and iii) an even larger delay for SKS. A crustal contribution to the variation of the relative teleseismic S and P delays is documented from the comparison of receiver-function and wide-angle reflection profiling of the Moho from the Himalayas into Qang Tang (Galvé et al., 2002b). Hence, part of the anisotropy causing the splitting with vertical slow axis could also be expected in the crust. This is also the kind of anisotropy that has been measured in western Europe for a region of reflective layered lower crust (Rabbel and Lueschen, 1996). S-waves from explosions propagate principally as SV since they result from interaction of the P waves generated with near source heterogeneities. In an anisotropic medium with a vertical slow axis, the SV-polarized wave is the fastest for wide-angle reflections that have incidence between 30° and 50°, where splitting is largest. At this incidence, V_p/V_s is then the lowest over the whole range of incidences and polarizations. For such a geometry, an apparent value of $V_p/V_s=1.57$ is measured in the case of very strong anisotropy of felsic schists (Godfrey et al., 2000) illustrating that such anisotropy could explain our calculated low V_p/V_s ratio. The V_p/V_s value representative of the schist composition is then of 1.73 (Godfrey et al., 2000). This value for the lower crust is still indicating a felsic nature.

In conclusion, even if we correct the V_p/V_s value from a possible anisotropy effect in the crust, we constrain low values of the average and lower crustal V_p/V_s in the Bayan Har block.

5. The northern Qang Tang block and transition to the Bayan Har block

5.1. Adapting survey design for sampling variations in structure

In the survey area, Yushu region is the boundary between the Qang Tang and the Bayan Har blocks. It comprises the Jinsha suture and the western part of the Xianshuihe strike-slip fault (Fig. 1). We were suspicious from past experiments that the technique of refraction and wide-angle reflection along across-strike profiles (Zhao et al., 2001) may not resolve correctly the sharp structural changes because of non-vertical, oblique rays interacting with them in a complex way. Thus, we resorted to additional propagation geometries such as broadside shooting with wide-angle reflection along strike and fan-recording at constant offset on a line across strike. In this case waves avoid structural variation along their path. Sharp traveltime changes that can be resolved along the fan-profile, then sample the variation across strike. Their structural significance could be checked by independent methods like vertical reflection profiles in the Pyrenees (Hirn, 1988; ECORS Pyrenees Team, 1988) or receiver-function profiles in southern Tibet (Hirn et al., 1984b; Galvé et al., 2002b). However across-strike transects do not resolve the velocity–depth distribution since waves are recorded at only one offset. It then exists in fan-profile images a trade-off between Moho depth variation and crustal velocity variation. Therefore we have the record-section of Shot 2 to north and we added south of the Jinsha suture a profile along the strike. These are the recording profile geometries from which a reliable velocity depth model can be obtained, since it complies best with the assumption of tabular structure, to correct from the velocity–depth variation of the structures above the Moho. Indeed, when placing Shot 1 broadside to the transect in order to achieve these geometries (Fig. 1), we also installed all available receivers on all roads and tracks in the region of Yushu (Shot 2). The area between the Jinsha suture and the Xianshuihe fault is so complex that it was likely to induce odd propagation of seismic waves blurring the image of deep interfaces, and we wanted to check this.

5.2. A low V_p/V_s for the whole crust south of the Jinsha suture, and a low velocity deeper crust to account for strong reflections from a deep Moho observed at short offset

On the reversed strike-line profile in the northern Qang Tang, the record-section of the profile northwestward from Shot 2 towards Shot 1 has the clearest wavefield (Fig. 2e). An unexpected result is that S-wave energy is present also for the Moho reflection. According to Galvé et al. (2002a), this observation supports the absence of significant partial melt. SmS arrival times, when compared to PmP (Fig. 6a), reveal that the whole crust has a low V_p/V_s ratio of

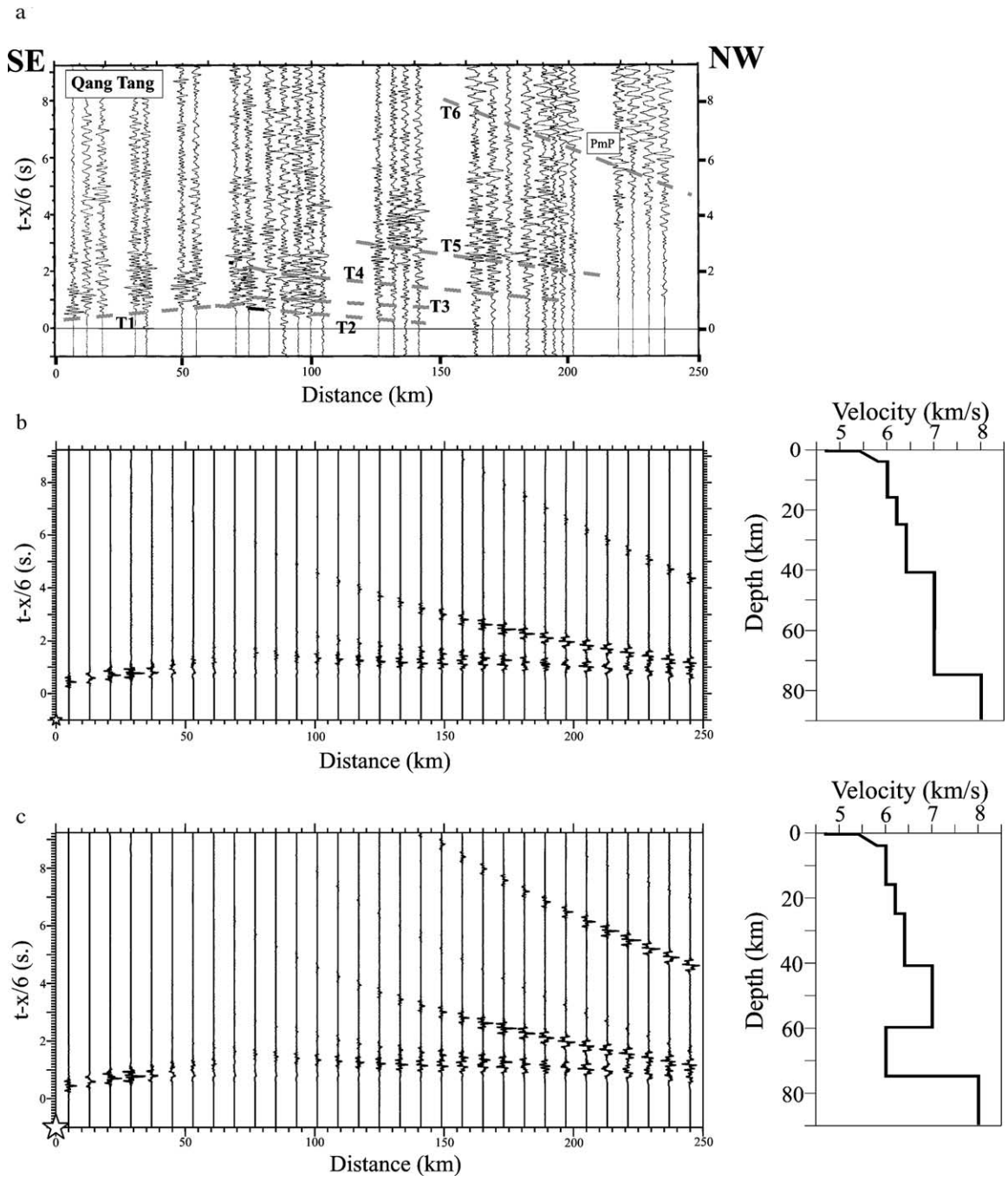

Fig. 6. Modelling of the strike-line in northern Qang Tang, Shot 2 towards NW. a) Observed record-section with a velocity reduction of 6 km/s, showing a strong Moho reflection T6 with strong amplitudes at short distance. b) Minimum structure model with layers of increasing velocity with depth accounting for traveltimes where observed. It does not allow to fit the amplitude and critical distance of the Moho reflection T6. c) Synthetic record-section for a model containing a low velocity layer on top of the crust–mantle interface. This option improves the fit of observations by bringing to higher amplitude at short offsets the Moho reflection T6.

1.73 ± 0.02. As in the Bayan Har block, this V_p/V_s value is indicative of a felsic crust.

By contrast, another observation illustrates a major difference with the Bayan Har (Fig. 2c and d). While in the Bayan Har block the difficulty was to account for a strong mid-crustal reflection, here it is the distance of the maximum of amplitude of the Moho reflection (Fig. 6a) that is not fitted by the minimum-structure model

(Fig. 6b), and a more complex one has to be considered. The rather short critical distance of ~140 km observed for the main intracrustal reflection T5 from the base of this 6.4 km/s layer (around 40 km depth) implies that the velocity underneath should be at least 7.0 km/s. However such a velocity all the way down to the crust–mantle boundary cannot account for the critical distance and the large amplitude observed for the Moho reflection. In order to model this feature in Fig. 6c, a velocity lower than 6.4 km/s has to occur between a mid-crustal high velocity layer and the Moho. A crustal thickness of 75 km is obtained with an average velocity of 6.26 km/s very abnormal with respect to any crustal average worldwide, which has important implications for the nature of the present crustal structure and its origin. This model with a low-velocity layer on top of the Moho increases the amplitude at short offset but still only fits approximately the distance of the maximum amplitude for the Moho reflection. It also provides no explanation for the observed low frequency of the Moho reflection with respect to the previous intracrustal reflection, which is discussed by Galvé et al. (2005—this issue) in terms of attenuation versus fine-layering.

For the sake of completeness, we note here that the reverse profile, from Shot 1, does not present the same clear character of deep reflections. Taken at face value in a 1D model, its not very clear PmP amplitude would lead to assume a small velocity contrast across the Moho, i.e., a higher value of velocity in the lower crust and hence a deeper Moho. However, the corresponding line of receivers at large offsets from Shot 1 had to straddle the suture to the east of Yushu, and reflection amplitude may here be affected by local heterogeneity, documented further hereafter.

5.3. Image of the deep crust: contrast in thickness across the Xianshuihe fault and possibly in crustal velocity across the Jinsha suture

Major and sharp variations of structure are indeed resolved across the boundary of Bayan Har to Qang Tang from a fan profile (Shot 1 recorded by the NNE–SSW main line, Fig. 1). In order to reach the large depth expected for the Moho in this area, recording was attempted at an offset of around 200 km. It was more successful than across the Kun Lun suture and fault, because Shot 1 here was more efficient than Shot 5 there. In Fig. 7, this depth-section is presented in which all the records displayed have been NMO-corrected and depth-transformed with the low average crustal velocity derived in the previous sections. We also introduce a central insert made of records from that Shot 2 to Shot 1 strike-line profile, with the high amplitude PmP.

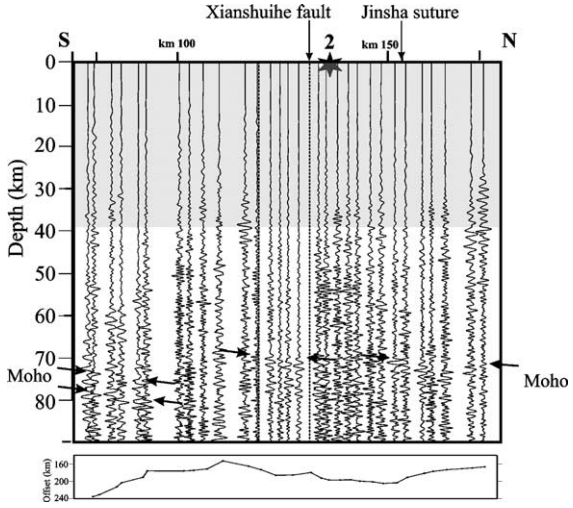

Fig. 7. Depth-converted record-section of wide-angle Moho reflections across the Bayan Har to Qang Tang. The central insert is data from Shot 2, the remainder from Shot 1, with recording offset indicated at the bottom. NMO correction of wide-angle to normal incidence times, and depth conversion assume the 6.26 km/s average crustal velocity obtained from modelling strike line from Shot 2. Grey area in top part recalls that depth transformation is only valid for the deep Moho reflections. Arrows indicate correlation of deep reflector, as two segments of Moho interface northdipping and southward downstepped with each other.

In Fig. 7, we can then correlate over the span of the depth-section two separate segments of the Moho interface that appear to be dipping northward. The northern Moho, around 70 km depth is sampled up to the south of the surface trace of the Jinsha suture and Xianshuihe fault. It is originally made of 2 segments that nearly connect (Fig. 7) at the Xianshuihe fault when we migrate the northern part of the record-section (north of the Xianshuihe fault) with the average velocity value of 6.35 km/s derived for the Bayan Har block.

A second Moho segment is hinted at on the record depth-section in its southern part, which samples south of the Xianshuihe fault well inside the Qang Tang which depth migration was done using the average crustal velocity of 6.26 km/s derived from Shot 2 in the northern Qang Tang. This short segment of Qang Tang Moho comes out more as a broad reflective zone and is at a great depth of 70–80 km, apparently dipping northward. The two segments of Moho interface can be followed on each side of the fan profile, although the late energy appear complex and not well correlated in space which can be due to propagation effects in a complex zone rather than weak reflector. From Shot 2 records, the strike-line profile south of

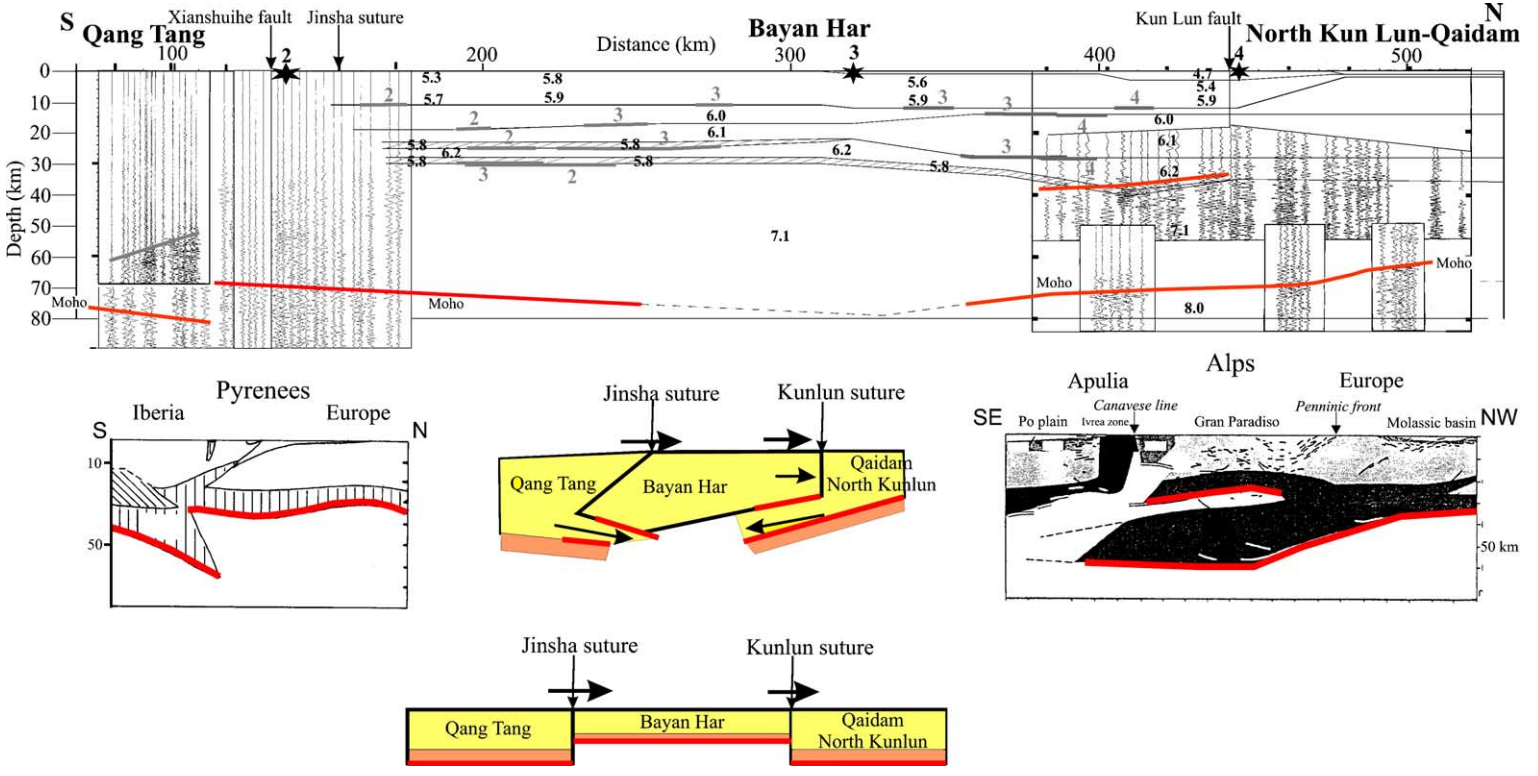

Fig. 8. Two dimensional crustal model for the Bayan Har and its borders, obtained by traveltimes modelling of three shots (numbered stars) along the transect. The 1D initial model for Bayan Har is the one in Fig. 4c, with the mid-crustal low velocity layer, and velocity in km/s is indicated for each layer. The thick grey lines represent the reflector segment points sampled for each shot which number is indicated. Superimposed are the NMO-corrected and depth converted seismograms from broadside recording on fan profiles, obtained across the Kunlun suture according to Galvé et al. (2002a) and Jinsha suture from Fig. 7, as described in the text. Moho has been highlighted in red. Inserts at bottom left and right, respectively are cartoons of lithospheric transects, with Moho highlighted in red, across the Pyrenes mountain range between France and Spain (Daignières et al., 1989), and the western Alps between France and Italy (here taken after Bayer et al., 1987). Insert at bottom center shows a schematical cartoon of possible evolution with time of the three blocks from before (bottom) to after (top) convergence due to the collision of India and northward motion as indicated by black arrows on top. Before collision, the Moho in red is beneath a layer of lower crustal lithology under the upper and intermediate crust in yellow and Moho depth is smaller beneath Bayan Har initially formed as a continent ocean margin sutured at the Jinsha suture after presumably southward subduction of its oceanic part in the Triassic–Jurassic. After convergence due to collision of India, the Bayan Har crust is schematized to have overridden the lower part of Qaidam crust, which seismic Moho may have migrated upwards by eclogitization of material of lower crustal, basic lithology. At its southern edge, the Bayan Har crust may have imbricated the thicker Qang Tang crust, which deeper part, of lower crustal more basic lithology may have been eclogitized with the seismic Moho having migrated upwards.

the suture indeed does not sample the deepest, southernmost Qang Tang Moho. In the transition from the main Bayan Har to Qang Tang blocks, at least two segments of Moho are identified, that are northdipping and southward downstepping with respect to each other. When the northern Moho and the deeper Qang Tang Moho are prolongated from the edges to the center of the section, they show an offset in depth that could be up to 20 km, if one was to believe in the southern broad Moho segment.

5.4. 2D crustal transect through Bayan Har and its edges, from traveltime modelling along section and broadside fan-profiling

Complementary elements of interpretation can be drawn from the structural variation along the NNE–SSW transect of the crustal section connecting the shotpoints in line (Fig. 8). This 2D model of interfaces and velocities is obtained by ray-tracing using the procedure of Zelt and Smith (1992) to adjust arrival times to observations for all direct and reverse overlapping record-sections.

Across the transition from Qang Tang to Bayan Har, the image of the Moho depth record-section of Fig. 7 discussed above has been superimposed. With respect to the ray-tracing traveltime modelling along the whole transect of Fig. 8, the northern Moho segment of Fig. 7 appears indeed as the southward geometrical continuation of the Bayan Har Moho modelled there. This Bayan Har Moho would hence extend further south than the location of the Jinsha suture at the surface. In the depth-section across the Qang Tang to Bayan Har in Fig. 8, the upper inset on the southern part is from records around 125 km offset that were designed to sample intracrustal interfaces, as had been the case across the Kun Lun fault (Galvé et al., 2002a). It highlights a reflector in the middle crust that is dipping southward into Qang Tang, away from the Jinsha suture.

This image of crust shows discontinuous Moho segments dipping northward under the transition zone, together with antithetic conjugate southward dipping of an intracrustal interface.

A similar case is recalled by the cartoon under this southern part of the transect, which represents the structure across the Pyrenean mountain belt between Spain and France which originated due to the Eocene convergence and strike-slip of the Iberian peninsula and Europe. Such a step in the Moho, highlighted in red, and crustal indentation with opposite vergence in the upper crust has been established by a succession of wide-angle reflection, teleseismic and vertical reflection methods (Hirn et al., 1980; Hirn et al., 1984c; ECORS Pyrenees Team, 1988).

The seismic-record depth-section superimposed on the north of the transect (Fig. 8) results from a fan-profile across the Kun Lun fault (Galvé et al., 2002a). It recalls the variation in crustal architecture, which was interpreted as resulting from the previously thinner crust of Bayan Har having thickened by thrusting over the lower crust of the North Kun Lun–Qaidam terrane. In front of it, the crustal thickening of the North Kun Lun–Qaidam occurred by the thickening of upper crustal material. In such a model of evolution, the strong reflector in the middle of the present Bayan Har crust that is not seen to the north of the Kun Lun fault, can be regarded as either the basal décollement, or as the Moho reflector of the previous Bayan Har material thrust over part of the North Kun Lun–Qaidam crust. This image can thus be interpreted in terms of this evolutionary model in any of the two alternative types of velocity–depth models of Bayan Har crust. Indeed depending on the option, the tectonic base of the Bayan Har unit that is thrust over to the north can be either within its former crust and thus give a reflective décollement, or beneath its Moho, which then is giving the strong reflections since they would dominate at wide-angle over those of any tectonic limit underneath.

As recalled by the cartoon beneath in Fig. 8, the position of the possible original base of the Bayan Har crust and that of the lower crust of the North Kun Lun that it overrides, which are sketched as Moho in red are similar to what is observed in the western Alps in the ECORS-CROP profile, from France to Italy (Nicolas et al., 1990; ECORS-CROP Deep Seismic Sounding Group et al., 1989). A similar, lithospheric wedging occurred there, not only which involved a sedimentary or crustal wedge, but also the lower crust and probably its upper mantle sole. These materials were thrown over the lower crust of the northwestern foreland, as sketched in the cartoon.

6. Conclusions and discussion

The seismic profiles reported here provide a representative sample of crustal wavefields for the three blocks of North–Central Tibet, constraining the variation of velocity with depth and sensing the horizontal variability of crustal structure. They evidence a contrast in internal structures among the three blocks crossed along this 700 km long transect, in terms of intracrustal reflectivity, and of composition, whereas the average crustal thickness, a parameter which may also be

approached by other methods, has modest variation except in the south.

Crustal thickness increases from 65 to 70 km and 80 km across block boundaries towards the centre of the Plateau. This is an abnormal thickness with respect to the continental average value of 41 km and the value of 46 km for orogens (Christensen and Mooney, 1995).

The second first-order parameter is the average crustal velocity resolved as being significantly different among blocks: on the order of $V_p = 6.2$ km/s for North Kun Lun–Qaidam, 6.36 km/s for Bayan Har, and 6.26 km/s for the northern edge of Qang Tang. These values are very low compared to continental or orogen average of 6.45 and 6.39 km/s, the more so when normal pressure and temperature derivatives are taken into account for the in situ conditions at the larger depth (Christensen and Mooney, 1995).

Another first-order parameter which is rarely constrained in explosion-seismic experiments is the velocity ratio V_p/V_s in the crust. In the North Kun Lun–Qaidam block, clear S-wave Moho reflections allowed us to constrain an average $V_p/V_s = 1.73 \pm 0.01$ (Galvé et al., 2002a). This is significantly lower than the average for a continental crust, which is 1.77 to 1.78 (Christensen and Mooney, 1995; Zandt and Ammon, 1995; Christensen, 1996). It hence documents an average felsic composition for the whole thickened crust. In the north Bayan Har, extremely low V_p/V_s is measured, smaller than 1.6 for the lower crust, anyway below 1.73 even if we take into account an anisotropy in the lower crust of the kind inferred in the lithosphere of the Lhasa block. In the north Qang Tang, the strike-line rather unexpectedly documents SmS that, although lacking sharpness yield a V_p/V_s ratio again as low as 1.73 ± 0.02.

These low V_p/V_s and V_p values constrain a felsic composition for the whole crust. Furthermore, in the intracrustal response obtained uniquely by explosion seismology resolves this not only on average but specifically for the lower half of the crust. The V_p/V_s values constrained as 1.73 and below are far less than the 1.77 value for the average crust (Christensen, 1996) that contains only an upper half of felsic material.

If the composition of the crust before thickening had been average, that is with about a lower half of basic and intermediate composition material, then an explanation of the absence of other than felsic velocities to 70 km depth is needed. This can be due to eclogitization of the basic part of the original crust in the crustal thickening process, which brings its velocity to mantle-like value, as discussed by Galvé et al. (2005—this issue). Such a process had been proposed to occur under the Himalayas and South Tibet up to the Indus–Tsangpo suture from the low V_p measured in the very thick crust (Hirn and Sapin, 1984; Sapin and Hirn, 1997). Such an explanation has also been resorted to by Beck and Zandt (2002) in order to account for the nature of the thickened orogenic crust in the Andes.

The seismic images of crustal architecture suggest mechanisms of lithospheric interaction in convergence. Crustal thickening appears to occur by two different mechanisms at the outboard and inboard of the Bayan Har in its northeastward motion towards stable Eurasia. We have indicated a possible analogy with the Alpine flat subduction and the Pyrenean lithospheric imbrication (Fig. 8), that we will place in the perspective of other models proposed for Tibet and its northeastern part.

The interaction between Bayan Har and North Kun Lun–Qaidam has been considered before by Tapponnier et al. (1990) and Meyer et al. (1998). Both studies emphasized the contrasting structures of upper crustal units and the sharp tectonic boundaries between them, and proposed a model of sequential growth and uplift of the plateau. Our seismic observations concur with this general view, but the particular form of their model of continental subduction may be discussed in a perspective to incorporate new elements.

In their analogy with subduction Tapponnier et al. (1990) and Meyer et al. (1998) predicted that the lower crust, Moho, and lower lithosphere of the North Kun Lun form a slab steeply dipping south and passing into the mantle beneath Bayan Har. They sketch the Moho of the subducting plate to be entrained to reach a depth of around 90 km under the 60 km deep Moho of the Bayan Har. Hence this model features a Moho step upward from north to south across the boundary. On the contrary a downward slope from north to south is shown in the cross-section obtained by explosion seismology (Galvé et al., 2002a, and Fig. 8). Furthermore with an independent method, a teleseismic receiver-function profile provides an image that Vergne et al. (2002) explicitly describe in terms of Moho steps located at the main sutures showing a crustal thickening that occurs in staircase fashion.

Rather than to lithospheric mantle subduction (Meyer et al., 1998) or to staircase-fashion southward-downstepping of the Moho (Tapponnier et al., 2001; Vergne et al., 2002), the cartoon of Tapponnier et al. (1990) taken at face value corresponds indeed to indentation of the North Kun Lun–Qaidam crust by the Bayan Har, that implies a mechanism of decoupling between the upper and the lower crust of Kun Lun–Qaidam. Such indentation with a décollement on top of the lower crust had been proposed earlier as part of the thickening process sug-

gested from seismic profiles by Hirn et al. (1984a,b,c) and Hirn (1984, 1988) through South Tibet–Himalayas, where they also proposed decoupling and interwedging in the mantle lithosphere.

Our seismic images show that the structure resulting from the convergence between North Kun Lun–Qaidam and Bayan Har presents features akin to subduction but with distinct differences. With respect to cartoon models of oceanic subduction, the slab which carries the North Kun Lun lower crust is imaged as dipping much flatter and underplating the Bayan Har much further. It is thus a flat subduction and only of part of the crust.

It is hence more reminiscent of the architecture that has been sketched for the Alps from seismic imaging (Nicolas et al., 1990; ECORS-CROP Deep Seismic Sounding Group et al., 1989). There similarly, lithospheric wedging and not only sedimentary or crustal wedging, but with certainly the lower crust and probably its upper mantle sole, have overridden the lower crust to the northwest. For the Alps, this northern continent is stable Europe with respect to the Apulian promontory whose crust overrides it and under which occurs flat partial crustal subduction. Similarly, we may describe here the southern unit (Bayan Har) as thrusting over the northern one, since the motion of Bayan Har is faster (Wang et al., 2001). However both units move to the north, which may cause the overthrust, or partial subduction of the crust of the North Kun Lun beneath to be flat.

Crustal thickening for each unit occurs either side of their contact at the surface in coupled processes but by different modes: superposition of Bayan Har crust on Kun Lun lower crust on one side and thickening of Kun Lun upper crust shoved off by the Bayan Har on the other.

In the transition between the Bayan Har and Qang Tang blocks, the Moho is made of at least two segments. These Moho segments are northdipping and southward downstepping with respect to each other. Together with the southward dip of a shallower intracrustal reflector, this gives an image of the lithospheric architecture with discontinuous Moho segments that may have been transported along a conjugate northdipping feature at depth. This picture suggests an interpretation in terms of thrusting of the upper part of the Qang Tang crust over the Bayan Har lithosphere which subducted under the Qang Tang in the Mesozoic, and the formation of an imbricated structure at Moho depth possibly in a more recent episode.

A northward overthrusting style at the surface may be inherited from the amalgamation of the two terranes in the Mesozoic, for which Kapp et al. (2003) suggest a very flat subduction of Bayan Har reaching far under Qang Tang. Post-collisional crustal thickening with the conjugate thrust at depth that would bring the southern, Qang Tang Moho to dip and deepen northward, downstepping under the Bayan Har Moho can be viewed as limited indentation of the Qang Tang by the Bayan Har crust.

Such antithetic lower crust imbrication is reminiscent of the Pyrenean mountain belt shown as an insert cartoon in Fig. 8. There, a thinner crust at the southern edge of Europe due to extension before convergence has similarly an initial asymmetry, being overridden by Iberia at the surface during convergence and strike-slip along the North Pyrenean fault. At depth however, the thicker Iberian crust partially subducts under the European crust, which appear as indenting it under the conjugate thrust at the surface (Hirn et al., 1980; ECORS Pyrenees Team, 1988). This structure has inspired the modelling of partial crustal subduction in orogens, as a classical example (Beaumont et al., 2000).

Notably, the Qang Tang Moho has a steep dip and does not reach far under the southern edge of Bayan Har, unlike the North Kun Lun Moho under the northern edge of Bayan Har. This style is then similar to that of the deep Iberian Moho of the thickened crust of the Pyrenees under the European crust to the north. These two cases with an initial asymmetry of a thicker crust in the southern plate result in partial and steep subduction of this thick crust, that is steep and does not reach far. This may be related to the other peculiarity they share, that the Moho of the thickened crust that subducts is in the plate, Iberia or Qang Tang which has the fast motion towards the other, Europe or Bayan Har.

Acknowledgements

This project was supported by the Department of International Cooperation, Science Technology, Ministry of Land and Resources, Beijing, the INSU-CNRS, the French Ministry of Research and Education, Paris and the French Embassy in Beijing. Discussions with Huang Chongli, Gao Ping and Chen Youfang are acknowledged. We also thank journal reviewers for their helpful suggestions to improve this paper.

References

Bayer, R., Cazes, M., Dial Piaz, G.V., Damotte, B., Elter, G., Gosso, G., Hirn, A., Lanza, R., Lombardo, B., Mugnier, J.L., Nicolas, A., Nicolich, R., Polino, R., Roure, F., Sacchi, R., Scarascia, S., Tabacco, I., Tapponnier, P., Tardy, M., Taylor, M.,

Thouvenot, F., Torreilles, G., Villien, A., 1987. Premiers resultants de la traversée des Alpes Occidentales par sismique réflexion verticale (Programme ECORS-CROP). C. R. Acad. Sci., Paris 305-II, 1461–1470.

Beaumont, C., Munoz, J.A., Hamilton, J., Fullsack, P., 2000. Factors controlling the Alpine evolution of the central Pyrenees inferred from a comparison of observations and geodynamical models. J. Geophys. Res. 105, 8121–8145.

Beck, S.L., Zandt, G., 2002. The nature of the orogenic crust in the central Andes. J. Geophys. Res. 107 (B10), 2230. doi:10.1029/2000JB000124.

Bruguier, O., Lancelot, J.R., Malavielle, J., 1997. U–Pb dating on single detrital zircon grains from the Triassic Songpan–Ganze flysch (central China): provenance and tectonic correlations. Earth Planet. Sci. Lett. 152, 217–231.

Chen, W.-P., Özalaybey, S., 1998. Correlation between seismic anisotropy and Bouguer gravity anomalies in Tibet and its implications for lithospheric structures. Geophys. J. Int. 135, 93–101.

Chen, W.-P., Chen, C.-Y., Nabelek, J.L., 1999. Present-day deformation of the Qaidam basin with implications for intra-continental tectonics. Tectonophysics 305, 165–181.

Christensen, N.I., 1996. Poisson's ration and crustal seismology. J. Geophys. Res. 102, 3139–3156.

Christensen, N.I., Mooney, W.D., 1995. Seismic velocity structure and composition of the continental crust: a global view. J. Geophys. Res. 100, 9761–9788.

Daignières, M., de Cabissole, B., Gallart, J., Hirn, A., Surinach, E., 1989. Geophysical constraints on the deep structure along the ECORS Pyrenees line. Tectonics 8 (5), 1051–1058.

ECORS-CROP Deep Seismic Sounding Group, Hirn, A., Nadir, S., Thouvenot, F., Nicolich, R., Pellis, G., Scarascia, S., Tabacco, I., Castellano, F., Merlanti, F., 1989. Mapping the Moho of the western Alps by wide-angle reflection seismics. Tectonophysics 162, 193–202.

ECORS Pyrenees Team, 1988. Deep reflection seismic survey across an entire orogenic belt: the ECORS Pyrenees profile. Nature 331, 508–511.

Fuchs, K., Mueller, G., 1971. Computation of synthetic seismograms with the reflectivity method and comparison with observations. Geophys. J. R. Astron. Soc. 23, 417–433.

Galvé, A., Hirn, A., Jiang, M., Gallart, J., De Voogd, B., Lépine, J.-C., Diaz, J., Wang, Y., Qian, H., 2002a. Modes of raising northeastern Tibet probed by explosion seismology. Earth Planet. Sci. Lett. 203, 35–43.

Galvé, A., Sapin, M., Hirn, A., Diaz, J., Lépine, J.-C., Laigle, M., Gallart, J., Jiang, M., 2002b. Complex images of Moho and variation of V_p/V_s across the Himalaya and south Tibet, from a joint receiver-function and wide-angle-reflection approach. Geophys. Res. Lett. 29 (24), 2182. doi:10.1029/2002GL015611.

Galvé, A., Jiang, M., Hirn, A., Sapin, M., Laigle, M., de Voogd, B., Gallart, J., Qian, H., 2005—this issue. Explosion seismic P and S velocity and attenuation constraints on the lower crust of the North–Central Tibetan Plateau, and comparison with South Tibet–Himalayas: implications on composition, mineralogy, temperature, and tectonic evolution. Tectonophysics 412, 141–157. doi:10.1016/j.tecto.2005.09.010.

Godfrey, N.J., Christensen, N.I., Okaya, D.A., 2000. Anisotropy of schists: contribution of crustal anisotropy to active source seismic experiments and shear wave splitting observations. J. Geophys. Res. 105, 27991–28007.

Hirn, A., 1984. Des géophysiciens sur le Toit du Monde. La Recherche 15, 878–881.

Hirn, A., 1988. Features of the crust–mantle structure of Himalayas–Tibet; a comparison with seismic traverses of Alpine, Pyrenean and Variscan orogenic belts. Philos. Trans. R. Soc., A 326, 17–32.

Hirn, A., Sapin, M., 1984. The Himalayan zone of crustal interaction: suggestions from explosion seismology. Ann. Geophys. 2, 123–130.

Hirn, A., Daignières, M., Gallart, J., Vadell, M., 1980. Explosion seismic sounding of throws and dips in the continental Moho. Geophys. Res. Lett. 7, 263–266.

Hirn, A., Lépine, J.C., Jobert, G., Sapin, M., Wittlinger, G., Xu, Z.X., Gao, E.Y., Wang, X.J., Teng, J.W., Xiong, S.B., Pandey, M.R., Tater, J.M., 1984a. Crustal structure and variability of the Himalayan border of Tibet. Nature 307, 23–25.

Hirn, A., Nercessian, A., Sapin, M., Jobert, G., Xu, Z.X., Gao, E.Y., Lu, D.Y., Teng, J.W., 1984b. Lhasa block and bordering sutures, a continuation of a 500 km Moho traverse through Tibet. Nature 307, 25–27.

Hirn, A., Poupinet, G., Wittlinger, G., Gallart, J., Thouvenot, F., 1984c. Teleseismic prospecting of lithospheric contrasts beneath the Pyrenees and Alps. Nature 308, 531–533.

Hirn, A., Jiang, M., Sapin, M., Diaz, J., Nercessian, A., Lu, Q.T., Lépine, J.-C., Shi, D.N., Sachpazi, M., Pandey, M.R., Ma, K., Gallart, J., 1995. Seismic anisotropy as an indicator of mantle flow beneath the Himalayas and Tibet. Nature 375, 571–574.

Hirn, A., Sapin, M., Lépine, J.-C., Diaz, J., Jiang, M., 1997. Increase in melt fraction along a south–north traverse below the Tibetan plateau: evidence from seismology. Tectonophysics 273, 17–30.

Hirn, A., Diaz, J., Sapin, M., Veinante, J.-L., 1998. Variation of shear-wave residuals and splitting parameters from array observations in southern Tibet. Pure Appl. Geophys. 151, 407–431.

Huang, W., Ni, J., Tilmann, F., Nelson, K.D., Guo, J., Zhao, W., Mechie, J., Kind, R., Saul, J., Rapine, R., Hearn, T., 2000. Seismic polarization anisotropy beneath the central Tibetan Plateau. J. Geophys. Res. 105, 27979–27989.

Kapp, P., Yin, A., Manning, C.E., Harrison, T.M., Taylor, M.H., Ding, L., 2003. Tectonic evolution of the Early Mesozoic blueschist-bearing Qiangtang metamorphic belt, central Tibet. Tectonics 22 (4), 1043. doi:10.1029/2002CT1383.

Kennett, B.L.N., 1975. The effect of attenuation on seismograms. Bull. Seismol. Soc. Am. 65, 1643–1651.

Kern, H., 1982. Elastic-wave velocity in crustal and mantle rocks at high pressure and temperature: the role of the high–low quartz transition and of dehydration reactions. Phys. Earth Planet. Int. 29, 12–23.

Kern, H., Richter, A., 1981. Temperature derivatives of compressional and shear wave velocities in crustal and mantle rocks at 6 kbar confining pressure. J. Geophys. 49, 47–56.

Mattauer, M., Malavieille, J., Calassou, S., Lancelot, J., Roger, F., Hao, Z., Xu, Z.Q., Hou, L.W., 1992. La chaîne Triasique de Songpan–Garze (Ouest Sechuan et Est Tibet): une chaîne de plissement-décollement sur marge passive. C. R. Acad. Sci. Paris 314, 619–626.

Métivier, F., Gaudemer, Y., Tapponnier, P., Meyer, B., 1998. Northeastward growth of the Tibet plateau deduced from balanced reconstruction of two depositional areas: the Qaidam and Hexi corridor basins, China. Tectonics 17, 823–842.

Meyer, B., Tapponnier, P., Bourjot, L., Métivier, F., Gaudemer, Y., Peltzer, G., Guo, S., Chen, Z., 1998. Crustal thickening in the Gansu–Qinghai, lithospheric mantle subduction, and oblique, strike-slip controlled growth of the Tibet Plateau. Geophys. J. Int. 135, 1–47.

Müller, H.J., Raab, S., 1997. Elastic wave velocities of granite at experimental simulated partial melting conditions. Phys. Chem. Earth 22, 93–96.

Nicolas, A., Hirn, A., Nicolich, R., ECORS-CROP Working Group, 1990. Lithospheric wedging in the western Alps inferred from the ECORS-CROP traverse. Geology 18, 587–590.

Owens, T.J., Zandt, G., 1997. Implications of crustal property variations for models of Tibetan plateau evolution. Nature 387, 37–43.

Rabbel, W., Lueschen, E., 1996. Shear wave anisotropy of laminated lower crust at the Urach geothermal anomaly. Tectonophysics 264, 219–233.

Sandvol, E., Ni, J., Kind, R., Zhao, W., 1997. Seismic anisotropy beneath the southern Himalayas–Tibet collision zone. J. Geophys. Res. 102, 17813–17823.

Sapin, M., Hirn, A., 1997. Seismic structure and evidence for eclogitization during the Himalayan convergence. Tectonophysics 273, 1–16.

Sobolev, S.V., Babeyko, A.Y., 1994. Modeling of mineralogical composition, density and elastic wave velocities in anhydrous magmatic rocks. Surv. Geophys. 15, 515–544.

Tapponnier, P., Meyer, B., Avouac, J.P., Peltzer, G., Gaudemer, Y., Guo, S., Xiang, H., Yin, K., Chen, Z., Cai, S., Dai, H., 1990. Active thrusting and folding in the Qilian Shan, and decoupling between upper crust and mantle in northeastern Tibet. Earth Planet. Sci. Lett. 97, 382–403.

Tapponnier, P., Xu, Z.Q., Roger, F., Meyer, B., Arnaud, N., Wittlinger, G., Yang, J., 2001. Oblique stepwise rise and growth of the Tibet plateau. Science 294, 1671–1677.

Vergne, J., Wittlinger, G., Qiang, H., Tapponnier, P., Poupinet, G., Jiang, M., Herquel, G., Paul, A., 2002. Seismic evidence for stepwise thickening of the crust across the north-eastern Tibetan plateau. Earth Planet. Sci. Lett. 203, 25–33.

Vergne, J., Wittlinger, G., Farra, V., Su, H., 2003. Evidence for upper crustal anisotropy in the Songpan–Ganze (northeastern Tibet) terrane. Geophys. Res. Lett. 30 (11), 1552. doi:10.1029/2002GL016847.

Wang, Q., Zhang, P.-Z., Freymueller, J.T., Bilham, R., Larson, K.M., Lai, X., You, X., Niu, Z., Wu, J., Li, Y., Liu, J., Yang, Z., Chen, Q., 2001. Present-day crustal deformation in China constrained by global positioning system measurements. Science 294, 574–577.

Wittlinger, G., Masson, F., Poupinet, G., Tapponnier, P., Herquel, G., Guilbert, J., Achauer, U., Xue, G.Q., Lithoscope Kunlun Team, 1996. Seismic tomography of northern Tibet and Kun Lun; evidence for crustal blocks and mantle velocity contrasts. Earth Planet. Sci. Lett. 139, 263–279.

Zandt, G., Ammon, C.J., 1995. Continental crust composition constrained by measurements of crustal Poisson's ratio. Nature 374, 152–154.

Zelt, C.A., Smith, R.B., 1992. Seismic traveltime inversion for 2-D crustal velocity structure. Geophys. J. Int. 108, 16–34.

Zhao, W., Mechie, J., Brown, L.D., Guo, J., Haines, S., Hearn, T., Klemperer, S.L., Ma, Y.S., Meissner, R., Nelson, K.D., Ni, J.F., Pananont, P., Rapine, R., Ross, A., Saul, J., 2001. Crustal structure of the central Tibet as derived from project INDEPTH wide-angle seismic data. Geophys. J. Int. 145, 486–498.

Zhu, L., Owens, T.J., Randall, G.E., 1995. Lateral variation in crustal structure of the northern Tibetan plateau inferred from teleseismic receiver functions. Bull. Seismol. Soc. Am. 85, 1531–1540.